Double Star Measures Using the Video Drift Method - XI

Richard L. Nugent
International Occultation Timing Association
RNugent@wt.net

Ernest W. Iverson
International Occultation Timing Association
ewiverson@consolidated.net

Abstract: Position angles and separations for 201 multiple star systems are presented using the video drift method. A method for measuring closer separations is presented that does not add additional optical elements into the light path. We present a technique for measuring double star systems that have a large magnitude difference.

Introduction

This is Paper XI in our continuing series on double star measurements using the video drift method first proposed by Nugent and Iverson 2011. We continue our practice of preferentially measuring multiple star systems in the Washington Double Star Catalog (WDS) that have not been measured for a minimum of 10-15 years and have fewer than 10 measurements.

Methodology

Measurements were made with a pair of Meade 14-inch LX-200 telescopes (focal length 3,556 mm at f/10, scale factor 0.6"/pixel). Multiple measurements were made for each double star system. Usually measurements were made over several nights but this was not always possible due to schedules and local weather conditions. Double star systems in which either the primary and/or secondary star is faint, image enhancement techniques were employed in capturing the raw video files. Co-author Iverson used the modified drift method employing an integrating video camera (Iverson and Nugent 2015) while co-author Nugent used a Collins I^3 image intensifier with and a non-integrating camera. Both telescopes were equipped with a UV-IR cutoff filter.

Combining Data and Reporting Errors

The standard drift method does not track the sky's movement but lets the double star drift across the field of view (FOV) while the telescope remains stationary (motor drive off). With the modified drift method, the telescope tracks the sky's movement (motor drive on) and the stars remain stationary. In the past we have referred to both types of data simply as a "drift". At best, this is confusing. For data reporting purposes we now use the term "sample" in place of "drift". In the standard case where the double stars are moving across the FOV, each complete drift is called a "sample". With the modified method, a 4-5-minute video clip is broken up into several "samples".

The *Limovie* software program is used to capture the component stars position as (x,y) coordinates referenced to the program's coordinate grid. The Excel software package, *VidPro* by author Nugent, uses these (x,y) coordinates pairs to compute the position angle and separation for each video frame. In the case of the standard sample, hundreds of video frames are used to compute the mean position angle (PA) and separation (SEP) for the sample. With the modified video drift method thousands of frames are used to compute the mean PA and SEP. *VidPro* also computes a standard deviation for the PA and the SEP that reflects the dispersion from the mean. Both random and systematic errors contribute to this dispersion. We attempted to minimize or eliminate known systematic errors, but many things contribute to the random error component. Perhaps the most significant is atmospheric motion. Incremental changes in the instantaneous optical path for the primary and secondary stars through the atmosphere make the stars appear to osculate slightly effecting their relative positions.

In our previous papers published in the JDSO, we combined the samples from a single night using a weighted average for the PA and SEP. When the dou-

ble star system was observed on multiple nights, the means from each night were combined again using a weighted average.

In the current study, a simple average is used to derive the mean PA and SEP each night. A standard deviation is calculated for each mean. The values from several nights are further combined, but this time using a weighted average. In cases where we both measured the same double star a weighted average was used to combine our respective measurements. We report these values in Table 2. The weight assigned to each measurement is simply the inverse of the standard deviation (from the nightly average) squared.

$$Weight = \frac{1}{\sigma^2} \quad [1]$$

Using this weight, a mean associated with a large standard deviation will contribute less to the weighted average than a measurement with a smaller standard deviation. We do not report the standard deviation in Table 2, but instead we report the Standard Error of the Mean (SEM), where *n* is the number of nights PA and SEP measurements were acquired:

$$SEM = \frac{\sigma}{\sqrt{n}} \quad [2]$$

In the special case where a double star was only observed on one night, we report the simple average of the *VidPro* position angle and separation for each "sample" from that night. The SEM is computed as before but uses the standard deviation calculated from the sample average and *n* is the number of samples.

Measuring Closer Separations

Our scale factor of 0.6"/pixel places limitations on the minimum separation we can measure. Under very good seeing conditions we can reach 6"-7" separations for doubles with similar component magnitudes. For close doubles with magnitude differences of $\Delta m \geq 1.5$ or more, the star images begin to merge making it difficult or impossible to measure and resolve a position angle and separation.

A common solution is to add a barlow lens or teleconverter lens into the optical path. Many observers do this. However, in any astrometric study, it's important to minimize the amount of glass between the camera sensor and the star. Extra lenses can potentially add unwanted distortions, aberrations and systematic errors. Persons in the field of astrometry have traditionally used mathematical models to correct for these distortions and aberrations, however each telescope's optical configuration requires a unique model.

Increased resolution can also be achieved by increasing the focal length of the telescope with extension tubes or decreasing the size of the camera sensor. Using a ¼-inch camera sensor in place of a ½-inch sensor will spread the star images over a larger area relative to the total image size. When *Limovie* displays the video, the star will be spread over more pixels thus increasing the apparent separation. This extra distance helps *Limovie* keep its aperture rings centered on the stars as they drift across the FOV. If the stars are too close, the aperture ring from the dimmer star will jump to the brighter star.

Instead of using one of these options, we increased the apparent focal length by adding a software magnification function to the Avisynth script used by *Limovie* to open the video file. The complete script is presented in Appendix 1. This script also allows the user to control the noise floor and apparent gain of the video.

A 2X magnification is preferred when using an integrating camera because the slightly longer sample time allows for more "new integrated" images to be captured. The 3X magnification version gives a slightly wider separation and is preferred when using a non-integrating camera.

At a 3X magnification, our scale factor resolution increases to about 0.2"/pixel and allows much closer separations to be measured. An example of the scale factor difference and resolution improvement for WDS 15077-3340 COO 288 is shown in Figure 1.

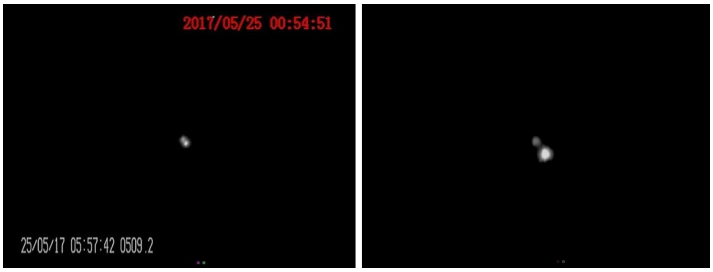

Figure 1. Left**:** *Full video frame of WDS 15077-3340 COO 288, 0.6"/pixel scale. The components are not resolved well enough for measuring.* Right: *Video frame segment with 3X magnification of same system, 0.2"/pixel scale. Components are better resolved for measuring. Our measured separation = 3.38".*

In this example, a single sample is partitioned into three individual segments for measuring: left, middle and right (See Figure 2). Each segment provides a separate position angle and separation measurement. But magnifying the video image is a two-edged sword – as the scale factor resolution increases (going from 0.6" to 0.2"/pixel), the effect of atmospheric motion also proportionally increases. Theoretically a video could be magnified to very high scale factors such as 0.1″/pixel and higher. This however will degrade the quality of the star images proportionally. We have found that with good atmospheric seeing, magnifying a video frame by a factor of three times its original size maintains a resolution adequate for measuring. Using this technique, we can measure double stars in the 3″ - 5″ separation range on nights with average seeing.

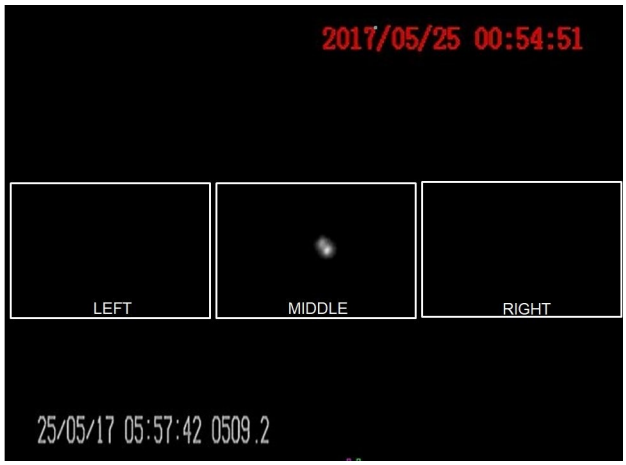

Figure 2. A 3X magnification factor will allow a sample to be broken up into left, middle and right segments. Each segment can be analized for the PA and SEP. For a 30 second video, each segment will be approximately 10 seconds in duration.

Defining the Segment Size

In a previous paper (Nugent and Iverson, 2014) we discussed the need for making a one-time aspect ratio adjustment to correct for anomalies in the video recording path. Once determined, the aspect ratio correction is used by an Avisynth filter to adjust the video's image size in *Limovie*. By convention we chose to set our horizontal aspect to 640 and vary the vertical aspect, as needed to accurately match the night sky. Changing the equipment attached to the rear of the telescope changes this ratio slightly. Therefore, author Nugent uses an aspect ratio of 640x485 pixels and author Iverson uses an aspect ratio of 640x471 pixels. For the 3X magnification example with author Nugent's equipment, each of the 3 equal segments has a width of 640/3 = 213 pixels (rounded). The height of each segment is set to an amount that maintains his previously calibrated aspect ratio of 640/485 = 1.32. In this case the height is set at 161 pixels.

Magnification Function Validation

We tested the magnification function on selected double star systems that were close to the lower resolution limit that could be measured reliably with and without magnification. The same samples were measured first with no magnification (0.6"/pixel resolution) and then at 3X magnification (0.2"/pixel resolution). The results are in Table 1.

Table 1. Comparison of measured PA's and separations from an unmagnified sample vs. a 3X magnified sample with 3 segments per sample. See text for explanation.

	Normal	3X Magnified		Normal	3X Magnified	
WDS	PA	PA	DIFF	SEP"	SEP"	DIFF"
02112-0233	347.1	347.5	-0.4	7.60	7.80	-0.20
03019-1633	314.4	314.3	0.1	7.10	7.10	0.00
03186+0827	356.8	356.5	0.3	5.40	5.50	-0.10
03351-1841	241.2	241.6	-0.4	7.30	7.20	0.10
04240-2259	353.3	354.1	-0.8	6.20	6.20	0.00
04289-2512	352.3	353.0	-0.7	6.90	6.90	0.00
04530-2758	224.5	224.6	-0.1	7.80	7.90	-0.10
05255+0250	307.4	307.7	-0.3	7.00	7.10	-0.10
13011-3337	238.1	237.0	1.1	4.80	4.90	-0.10
13377-1444	261.1	260.0	1.1	4.90	5.10	-0.20
02171+3727	9.6	9.5	0.1	7.92	7.90	0.02
01400+2611	232.8	232.8	-0.1	7.80	7.80	0.00
02501+0138	270.0	269.9	0.0	8.44	8.45	-0.01
03038+3529	222.7	222.8	-0.2	8.30	8.16	0.14
		Avg. Diff	0.40			0.08

The average difference for PA's for normal vs. magnified videos for the test doubles was 0.40°. The average difference for SEP's for normal vs. magnified videos was 0.08". We are confident that using the magnification function on the videos is reliable and does not add a systematic error. The one minute YouTube video clip, https://www.youtube.com/watch?v=bUxE4PtgOaA&feature=youtu.be illustrates the atmospheric issues discussed using a normal video vs. a magnified video.

Measuring Systems with Large Magnitude Differences

Normally measuring a double star with a large magnitude difference between the components is difficult and the measurement is subject to increased uncer-

tainty. Daley 2007 described a method using a small strip of solar film acting as an occulting bar to selectively block the brighter star and reduce its glare. *Limovie* can be adapted to measure double stars with a large magnitude difference by taking advantage of the program's ability to find the star's centroid and not the maximum amplitude. *Limovie*'s (*x*,*y*) coordinate measuring feature requires its apertures rings to fit completely over the star's image. If the star is bright and its image is larger than *Limovie*'s aperture rings an accurate centroid cannot be obtained. Saturation does not degrade the centroid as long as the star is completely within the aperture rings. Limovie finds the centroid of the star through the luminance cone surrounding the stars position and is not based on the maximum amplitude. Any pixel in this cone with a luminance value of at least 50% of the maximum value is assumed to be part of the star image, and the center of gravity of these pixels is recorded as a center of the star. The 50% threshold value is user adjustable.

Take the case of WDS 04095-1729 BUP 50AC. Its magnitudes are: primary component **A**, *m* = +8.07, secondary component **C**, *m* = +14.2. Its POSS-II image is shown in Figure 3, left frame. This 6+ mag difference makes it impossible to use *Limovie* to see both the primary and secondary components simultaneously at the same brightness level. The problem occurs when the brightness level is set high enough to see the secondary it makes the image of the primary too large (Figure 3, middle frame) to allow *Limovie's* aperture rings (shown) to fit over it. With the brightness level set low enough for the aperture ring to fit over the primary, then the secondary cannot be seen. *Limovie's* aperture rings have a 50-pixel maximum size (see Figure 3's middle and right frames).

The solution to this problem is to run the video through *Limovie* twice. The Avisynth "level" filter allows adjustments to the video brightness level during the analysis procedure (see Appendix 1 and Iverson and Nugent 2015 for a discussion of its use). The first run has the video brightness set high enough to see the **C** component with an adequate SNR and allow *Limovie*'s aperture to fit over it. The output .csv data file from this run will include the (*x*,*y*) coordinates for the **C** component.

The second run must use the exact same video frames (determined by the *Limovie* frame counter – See Figure 4) but this time the video brightness is set low enough to make the primary **A** star image small enough to allow *Limovie*'s aperture to fit over it. The output .csv data file from this run will include the (*x*,*y*) coordinates for the **A** component.

The final step is to combine the (*x*,*y*) coordinates from one .csv into the other .csv file using "cut and paste". For example, the (*x,y*) position data from the **C** component .csv file should be copied into the (*x,y*) columns reserved for the second object in the **A** component .csv file. The goal here is to have a single .csv file that contains the (*x,y*) coordinates from both runs. The combined .csv file is processed normally by *VidPro*.

Acknowledgements

This research makes use of the *Washington Double Star Catalog* maintained at the US Naval Observatory. We acknowledge the use of the Second Palomar Observatory Sky Survey (POSS-II) was made by the California Institute of Technology with funds from the National Science Foundation, the National Geographic Society, the Sloan Foundation, the Samuel Oschin Foundation, and the Eastman Kodak Corporation.

(Text continues on page 575)

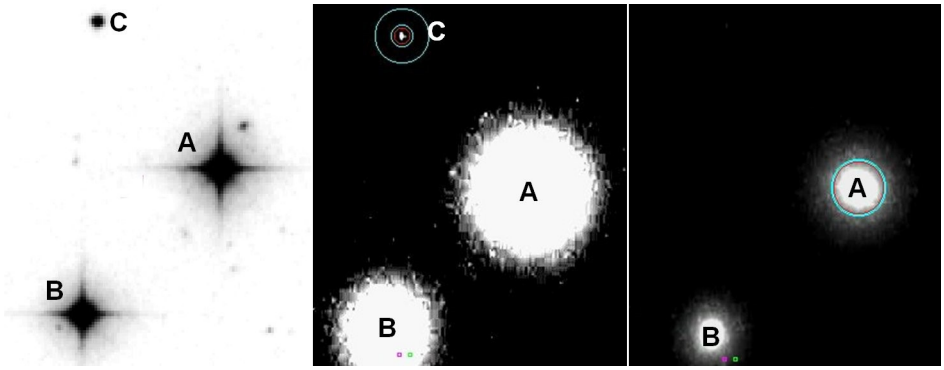

*Figure 3. WDS 04095-1729 BUP 50AC. Left frame: POSS-II image. Middle frame: Limovie video brightness set very high to see the secondary **C** component thus the primary **A** is excessively large. Limovie's outer aperture ring is 50 pixels wide. Right frame: Video brightness set low enough to allow Limovie's aperture ring to fit over the **A** component.*

Double Star Measures Using the Video Drift Method - XI

Table 2. Results of 201 double stars using the video drift method.

			PA		Sep.					
Object	Designation	PA°	SEM°	Sep"	SEM"	Avg. Date	Mag. 1	Mag. 2	Samples	Nights
00185+2608	STF 24	246.6	0.130	5.12	0.011	2017.86	7.79	8.44	17	4
00199-2011	ARA 824	293.8	2.143	10.54	0.396	2017.95	9.93	12.9	2	1
00345-0433	ALL 1AB,D	159.2	0.051	204.59	0.191	2017.79	7.10	9.99	5	1
00345-0433	STF 39AB,C	45.2	0.010	19.60	0.170	2017.78	7.10	8.65	27	6
00345-0433	ALL 1AB,D	158.7	0.071	200.77	0.298	2017.87	7.10	9.99	4	1
00408-0714	STF 49	320.2	0.060	8.60	0.010	2017.83	7.12	9.98	12	3
00518-0810	STF 68AB,C	295.0	0.010	7.75	0.003	2017.83	8.31	9.91	25	6
00529+1316	UC 454	94.3	2.164	11.77	0.527	2017.95	12.2	14.0	2	1
00586+0457	HDO 41	303.4	1.044	6.83	0.141	2017.87	11.98	12.7	6	1
01007+0929	DOO 25AC	214.2	0.233	74.46	0.332	2017.87	8.78	11.87	2	1
01007+0929	DOO 25CD	196.8	1.711	10.59	0.318	2017.87	11.86	11.87	2	1
01044-0518	STF 85AB	158.6	0.010	36.97	0.014	2017.83	8.71	10.57	29	6
01044-0518	STF 85AC	122.3	0.010	38.10	0.004	2017.83	8.71	12.09	21	6
01044-0518	STF 85BC	53.2	0.010	23.28	0.004	2017.83	10.57	12.09	21	6
01048-0528	BU 1356AC	37.2	0.003	107.53	0.008	2017.84	8.80	11.9	15	5
01048-0528	STF 86AB	137.2	0.028	16.84	0.008	2017.84	8.80	9.20	25	5
01052+1250	HJ 10AB	313.5	0.017	4.97	0.005	2017.85	9.60	10.50	17	5
01052+1250	HJ 10AC	57.8	0.009	8.86	0.002	2017.80	9.6	10.5	19	5
01052+1250	HJ 10BC	82.9	0.027	11.19	0.003	2017.85	10.50	10.50	12	4
01057+2128	STF 88AB	159.3	0.020	29.84	0.008	2017.88	5.27	5.45	32	7
01057+2128	STF 88AC	123.7	0.003	90.42	0.003	2017.85	5.27	10.71	18	6
01057+2128	STF 88BC	109.0	0.010	68.46	0.005	2017.85	5.45	10.71	15	5
01084+0539	STT 552AC	123.7	0.134	179.69	0.484	2017.88	5.52	11.09	2	1
01155-4549	CPO 109AB,C	95.3	2.001	9.34	0.200	2017.87	9.80	10.7	3	1
01171-1855	HJ 2034	153.3	2.132	9.15	0.336	2017.87	11.7	11.5	2	1
01221-0150	BAL 5	307.1	2.100	7.75	0.297	2017.87	11.19	12.9	2	1
01226-0348	HJ 637	186.8	0.576	29.62	0.301	2017.87	7.75	13.8	2	1
01240+1950	HO 309AC	93.4	0.792	47.39	0.686	2017.88	8.42	13.53	2	1
01244+2403	POU 125	325.3	1.806	4.65	0.133	2017.95	13.6	14.0	9	1
01270+3740	ES 2548	172.5	1.741	6.05	0.159	2017.95	11.5	12.0	6	1
01285+3708	ES 2009	275.9	1.485	4.75	0.130	2017.95	12.62	12.84	6	1
01305-1734	B 2516	94.4	0.482	5.58	0.061	2017.87	9.74	11.71	6	1
01308-2138	ARA1609	304.4	2.638	7.17	0.392	2017.87	12.6	12.8	2	1
01347+0502	SKF 4AB	130.4	1.057	17.12	0.371	2017.87	11.8	13.0	2	1
01381+2447	POU 135	215.5	1.073	5.06	0.103	2017.95	11.84	13.8	7	1
01400+2611	UC 16	232.8	2.581	7.80	0.336	2017.95	11.22	13.65	2	1
01400-1348	GAL 311AB	29.4	0.008	32.29	0.005	2017.86	10.95	11.01	20	6
01400-1348	GAL 311AC	216.9	0.023	6.50	0.003	2017.86	10.95	14.00	18	6
01422+2350	POU 141	67.9	1.483	5.77	0.151	2017.95	12.6	14.1	9	1
01432-2137	HJ 3456AB	352.7	0.940	14.96	0.272	2017.87	8.34	10.33	2	1
01434-2310	B 22	293.5	0.954	5.22	0.099	2017.87	9.72	11.39	6	1
01474+0355	HJ 2084	332.1	0.469	17.64	0.212	2017.87	9.4	12.8	3	1
01477+2358	POU 145	323.1	2.107	9.16	0.361	2017.95	11.0	13.4	2	1
01487+0741	HJ 644AB	279.3	0.534	17.20	0.219	2017.87	7.18	11.7	2	1

Table 2 continues on the next page.

Double Star Measures Using the Video Drift Method - XI

Table 2 (continued). Results of 201 double stars using the video drift method.

			PA		Sep.					
Object	Designation	PA°	SEM°	Sep"	SEM"	Avg. Date	Mag. 1	Mag. 2	Samples	Nights
01487+0741	HJ 644AC	226.8	0.166	126.52	0.435	2017.87	7.18	9.90	2	1
01487+0741	FOX9042AD	123.6	0.286	77.58	0.467	2017.87	7.18	11.60	2	1
01489-3153	LDS3316	56.3	1.105	6.21	0.113	2017.87	10.98	13.02	6	1
01506+0231	HDO 54AB	117.7	0.906	4.45	0.080	2017.87	9.82	11.0	9	1
01506+0231	HDO 54AC	214.0	1.435	17.15	0.308	2017.87	9.82	12.83	3	1
01506+0231	ABT 1AD	208.6	0.403	69.95	0.344	2017.87	9.82	12.83	3	1
01528+4016	MLB 999	5.8	1.329	4.29	0.100	2017.95	11.5	12.0	9	1
01536+3758	BRT2199	217.6	1.665	3.96	0.101	2017.95	12.37	13.14	9	1
01567+3749	ES 161	244.5	0.810	3.89	0.050	2017.95	10.49	11.7	9	1
01575-2045	ARA1258	336.8	3.263	7.93	0.428	2017.87	11.72	13.1	2	1
02004-0831	HJ 3476AB	202.1	0.370	61.48	0.239	2017.87	5.66	11.39	3	1
02018-2221	ARA1612	128.5	1.914	5.77	0.202	2017.95	12.7	13.0	8	1
02021+0355	OSV 1	15.7	1.110	17.64	0.346	2017.95	10.70	13.39	2	1
02058+3800	ES 2010	137.2	0.379	9.17	0.065	2017.95	9.2	12.1	4	1
02112-0233	DAM1002	347.1	3.865	7.61	0.387	2017.87	13.4	13.8	3	1
02116-1049	SKF 351	75.6	1.394	4.56	0.120	2017.87	11.6	12.3	6	1
02144+3734	ES 2011	343.2	1.029	4.31	0.061	2017.95	11.30	12.8	9	1
02163-0949	ARN 30AC	221.1	0.004	260.23	0.014	2017.89	6.98	9.64	9	3
02163-0949	STF 242AB	249.2	0.007	80.09	0.008	2017.90	6.98	11.29	17	5
02171+3727	ALI 264	9.5	2.560	7.90	0.301	2017.95	13.2	13.4	2	1
02189+2529	POU 172	147.3	3.581	9.48	0.605	2017.95	13.0	14.4	2	1
02222+2437	POU 180	159.3	2.280	12.06	0.431	2017.95	12.46	14.3	2	1
02233-0749	HO 313AC	74.7	0.940	17.62	0.290	2017.87	9.48	13.26	2	1
02240-0752	HO 314AC	347.3	0.484	67.86	0.583	2017.87	9.45	12.48	2	1
02247-2002	FAL 76AC	203.4	0.898	17.77	0.279	2017.87	8.93	11.14	2	1
02255-3956	WG 13	0.9	1.847	8.60	0.281	2017.87	11.6	12.9	3	1
02273+3715	ALI 265	159.7	2.231	8.73	0.279	2017.95	10.95	12.6	2	1
02320+1743	HJ 2145AB	223.8	2.153	15.00	0.544	2017.87	11.59	13.8	2	1
02320+1743	HJ 2145AC	296.0	1.365	26.49	0.697	2017.87	11.59	14.6	2	1
02342-3131	HJ 3509AB	58.8	0.771	23.22	0.308	2017.87	7.63	11.34	2	1
02366-1654	FEN 2	333.1	2.266	4.69	0.193	2017.95	13.0	13.1	6	1
02405-1341	GAL 324AB	74.9	0.636	42.43	0.499	2017.95	10.48	12.48	2	1
02424+2001	BU 522AB	264.6	0.156	18.63	0.145	2017.87	5.69	12.2	2	1
02501+0138	BAL1257	270.0	1.418	8.44	0.361	2017.95	11.08	12.47	2	1
02566+3620	ALI 44	209.5	1.669	14.95	0.346	2017.95	11.0	12.2	2	1
02570+1848	GRV 153	276.8	2.641	7.60	0.371	2017.87	11.8	12.4	2	1
03019-1633	RST2292AB	314.4	1.846	7.10	0.269	2017.87	11.2	11.8	2	1
03024+2633	J 1083AC	190.8	0.629	13.77	0.129	2017.95	9.3	13.0	9	1
03038+3529	ALI 45	222.7	2.227	8.30	0.265	2017.95	12.0	12.6	2	1
03041+3509	POP 11AB	333.6	2.963	10.88	0.438	2017.95	13.1	13.6	2	1

Table 2 continues on the next page.

Double Star Measures Using the Video Drift Method - XI

Table 2 (continued). Results of 201 double stars using the video drift method.

			PA		Sep.					
Object	Designation	PA°	SEM°	Sep"	SEM"	Avg. Date	Mag. 1	Mag. 2	Samples	Nights
03124+3500	HO 501	205.6	0.372	9.17	0.048	2017.95	8.80	12.1	3	1
03127-0254	HJ 3554	353.0	0.012	21.41	0.005	2017.88	8.82	10.09	22	6
03141+3518	POP 71	105.9	1.133	5.05	0.103	2017.95	11.2	12.7	6	1
03186+0827	SKF 482AB	356.6	2.563	5.28	0.336	2017.87	13.3	14.5	2	1
03322+2406	POU 292	238.4	4.932	10.05	0.803	2017.95	13.3	13.9	2	1
03333+2515	POU 294	171.8	3.087	11.18	0.583	2017.95	11.16	14.40	2	1
03340+2348	POU 296	206.3	3.695	10.10	0.590	2017.95	12.4	13.8	2	1
03348-2531	UC 1025	46.4	2.542	10.17	0.424	2017.95	9.8	11.0	2	1
03351-1841	ARA 525	241.3	2.652	7.35	0.336	2017.95	10.45	12.1	2	1
03402+2820	UC 1039AB	3.4	1.329	11.70	0.429	2017.95	13.4	13.4	3	1
03430+3658	ALI 286AB	341.3	1.421	13.65	0.325	2017.95	9.67	12.6	2	1
03430+3658	ALI 286AC	172.5	1.640	9.38	0.216	2017.95	9.67	12.7	2	1
03468+3049	HJ 665AC	260.8	1.089	14.65	0.279	2017.95	10.53	12.26	2	1
03543-0257	STF 470AB	348.2	0.009	6.87	0.003	2017.89	4.80	5.89	31	7
03543-0257	STF 470AC	4.5	0.008	164.71	0.017	2017.93	4.80	10.50	15	5
03551+2352	POU 315	310.9	2.941	6.91	0.404	2017.95	12.7	13.0	3	1
03586-0239	BU 1042A,BC	91.1	0.009	59.01	0.017	2017.93	7.72	10.07	35	7
03586-0239	BU 1042AD	250.8	0.004	37.29	0.005	2017.93	7.72	13.26	21	7
04362+0913	STF 569	134.4	0.020	7.99	0.004	2017.96	8.74	9.56	30	6
04552+0058	BAL 976	138.5	0.017	6.14	0.002	2017.94	9.95	10.16	28	6
05133+0252	STF 654AB	65.2	0.087	6.44	0.029	2018.00	4.62	8.50	11	3
05133+0252	STF 654AC	157.0	0.005	183.39	0.004	2017.99	4.62	11.43	6	2
06282+0516	STF 915AB	43.1	0.047	5.85	0.008	2017.98	7.60	8.52	20	4
06282+0516	STF 915AC	128.8	0.054	39.59	0.027	2017.96	7.60	11.78	6	2
06296+0542	SLE 287	209.3	0.039	8.55	0.009	2017.98	9.54	9.80	16	4
06317+0546	STF 926AB	287.4	0.031	10.79	0.006	2017.98	7.23	8.62	20	4
07047+0556	HJ 2360	150.5	0.045	16.30	0.016	2018.00	8.00	9.41	15	3
10198-2459	J 1564	122.7	1.818	4.95	0.186	2017.32	10.0	11.2	6	1
12018-2504	B 2736A,BC	316.7	1.146	40.95	0.612	2017.39	9.49	13.92	2	1
12019-4100	WG 148	290.7	2.485	7.42	0.269	2017.40	11.52	12.4	2	1
12035-3655	HJ 4499	44.5	2.376	7.62	0.272	2017.40	10.17	10.45	2	1
12053-3511	LDS 854	115.6	0.495	27.56	0.251	2017.40	10.69	13.43	2	1
12061-3258	HJ 4495AC	45.5	0.350	45.95	0.286	2017.40	6.69	12.88	2	1
12141-3644	SEE 147AB,C	306.0	0.880	27.72	0.417	2017.39	8.53	11.72	2	1
12162-4112	WG 151	55.6	2.285	7.85	0.238	2017.40	11.6	11.8	4	1
12163-2706	HJ 4509CD	288.4	2.600	8.10	0.294	2017.39	12.6	13.6	3	1
12190-2253	RSS 285	310.8	0.764	18.06	0.308	2017.39	9.20	12.0	2	1
12226-3103	LDS 407	40.1	4.120	9.79	0.516	2017.39	14.0	14.4	3	1
12242-3224	HJ 4519AB	91.2	1.900	8.83	0.337	2017.39	9.8	11.4	3	1
12267-2850	FOX 174	310.8	2.284	12.69	0.636	2017.39	9.6	12.1	2	1

Table 2 continues on the next page.

Double Star Measures Using the Video Drift Method - XI

Table 2 (continued). Results of 201 double stars using the video drift method.

			PA		Sep.					
Object	Designation	PA°	SEM°	Sep"	SEM"	Avg. Date	Mag. 1	Mag. 2	Samples	Nights
12269-3728	HJ 4510AB	42.7	1.369	19.52	0.371	2017.39	9.73	10.38	3	1
12269-3728	HJ 4510BC	14.0	2.434	12.12	0.329	2017.39	10.38	10.43	3	1
12269-3728	HJ 4510BD	301.1	1.732	16.30	0.400	2017.39	10.38	13.5	2	1
12340-2312	DON 537A,BC	76.1	1.273	14.93	0.371	2017.39	10.6	11.1	2	1
12349-3125	B 2296	69.7	1.549	12.40	0.290	2017.40	9.1	14.	2	1
12434-2514	I 908AC	21.2	0.732	39.78	0.502	2017.39	10.22	12.15	2	1
12434-2514	B 2739CD	294.6	3.461	7.66	0.449	2017.39	12.2	13.9	2	1
12485-2426	ARA2183	222.3	3.444	7.97	0.502	2017.39	12.7	12.7	2	1
12517-3321	SEE 164AC	112.7	0.983	41.80	0.615	2017.40	8.77	14.67	2	1
12524-3319	PRO 103	335.0	4.150	7.69	0.435	2017.39	10.7	10.7	3	1
12539-3310	I 910AB	35.9	0.400	52.85	0.301	2017.40	8.66	10.63	2	1
12597-0349	STF1704AB	53.7	0.735	20.57	0.286	2017.40	5.80	10.3	2	1
13011-3337	HJ 4563	238.1	2.210	5.87	0.237	2017.39	7.02	8.23	2	1
13016-2440	B 2306	76.7	0.813	11.55	0.191	2017.40	7.25	13.5	2	1
13021-2224	B 1726A,BC	157.8	0.944	15.33	0.262	2017.40	9.77	10.99	2	1
13024-3125	DAW 165AC	78.7	0.852	23.87	0.304	2017.40	10.43	12.5	2	1
13058-0503	A 10CD	58.7	0.891	19.30	0.286	2017.40	10.2	12.0	2	1
13089-0148	GWP1921AB	167.1	1.177	25.38	0.470	2017.40	10.6	14.7	2	1
13094-0006	GWP1923	143.8	1.418	10.77	0.315	2017.40	8.0	10.9	2	1
13099-0532	H 6 43AC	300.3	0.205	71.63	0.286	2017.40	4.40	10.4	2	1
13099-0532	H 6 43BC	296.8	0.011	66.72	0.021	2017.40	9.4	10.4	2	1
13129-0213	GWP1939AC	226.3	0.110	237.04	0.302	2017.40	11.2	7.5	3	1
13130-2906	HWE 27AC	280.7	0.831	38.63	0.488	2017.39	8.03	13.45	2	1
13141-3215	HJ 4574AB	154.5	1.545	20.77	0.513	2017.39	9.2	12.8	2	1
13149-1122	SHJ 162AB	45.0	0.187	113.16	0.385	2017.40	7.11	8.18	2	1
13185-3206	SEE 175AC	113.1	0.764	41.05	0.488	2017.40	9.16	14.00	2	1
13203-0140	PWS 5AC	307.5	0.216	135.32	0.562	2017.40	11.60	12.38	2	1
13203-0140	PWS 5BD	250.1	0.774	35.46	0.651	2017.40	13.42	13.45	2	1
13208+0701	MNK 1AB	52.2	1.842	17.68	0.559	2017.40	10.29	12.90	2	1
13225-2257	ARG 26AB	79.8	0.523	27.45	0.258	2017.40	8.13	8.32	2	1
13239-2346	ARA2185	234.1	1.973	9.09	0.297	2017.40	11.3	12.5	2	1
13242-1844	UC 2531	320.6	3.154	10.68	0.721	2017.40	11.3	14.7	2	1
13242-2228	B 2314	30.5	1.432	7.59	0.194	2017.40	9.26	13.1	2	1
13263-3959	WG 164AC	272.3	0.824	26.34	0.346	2017.40	9.49	10.28	2	1
13270-2021	B 2751AB	108.4	1.301	15.95	0.382	2017.40	9.27	11.9	2	1
13377-1444	BU 611AB	262.2	0.935	4.82	0.167	2017.40	9.54	13.0	3	1
13385-1450	HJ 2666	187.7	1.810	12.59	0.375	2017.40	10.06	13.89	2	1
13394-1921	BHA 59AB	168.4	0.785	20.43	0.265	2017.40	13.26	12.49	2	1
13394-1921	TOB 253AC	45.5	0.997	23.10	0.389	2017.40	13.26	13.57	2	1
13408-2815	HO 382AB	358.5	0.824	13.79	0.226	2017.40	8.08	12.6	2	1

Table 2 concludes on the next page.

Double Star Measures Using the Video Drift Method - XI

Table 2 (conclusion). Results of 201 double stars using the video drift method.

			PA		Sep.					
Object	Designation	PA°	SEM°	Sep"	SEM"	Avg. Date	Mag. 1	Mag. 2	Samples	Nights
13490-2822	BU 413	106.0	0.325	66.83	0.343	2017.40	7.79	9.59	2	1
14176-2750	HWE 31	71.2	1.371	5.36	0.126	2017.40	9.51	9.89	6	1
15077-3340	COO 288	34.6	1.469	3.38	0.064	2017.40	9.69	10.15	3	1
15090-2024	B 1774	328.4	2.236	4.95	0.171	2017.40	9.39	11.6	3	1
15230-2326	DON 731	85.8	2.064	4.09	0.121	2017.40	10.06	11.8	3	1
16121+1155	STF2016	148.1	0.075	7.56	0.009	2017.55	8.49	9.60	5	1
18009+2633	STF2263	159.9	0.059	7.78	0.011	2017.55	8.73	9.93	5	1
18523+1432	WAL 97AC	87.9	0.033	60.07	0.017	2017.55	6.63	11.01	3	1
18523+1432	WAL 97AD	118.5	0.033	84.12	0.003	2017.55	6.63	10.9	3	1
18540+1516	L 40	6.3	0.096	12.89	0.023	2017.55	8.56	11.7	5	1
19041+1447	STF2443	310.8	0.097	6.81	0.005	2017.55	8.93	9.30	5	1
21221+1948	STFB 11AB	310.5	0.037	35.82	0.034	2017.78	4.20	9.3	20	4
21221+1948	STFB 11AC	13.0	0.088	64.34	0.132	2017.81	4.20	12.9	3	1
21374+2340	HJ 1668	37.1	0.077	7.85	0.010	2017.78	9.04	10.44	13	3
21389+3623	STF2814	160.5	0.190	8.32	0.049	2017.80	8.77	9.87	10	2
22305-0807	STF2913	327.9	0.022	8.04	0.004	2017.78	7.78	8.60	23	5
23100+3651	S 825AB	318.4	0.016	67.46	0.017	2017.82	7.78	8.26	25	5
23135-3329	SKF1255	240.0	2.086	16.38	0.537	2017.87	11.0	12.0	2	1
23228+2034	STF 3007AC	304.6	0.014	103.80	0.012	2017.82	6.74	10.86	17	5
23238-0828	STF3008	147.4	0.028	7.05	0.003	2017.78	7.21	7.67	25	5
23384-1939	ARA1248	137.8	1.780	7.18	0.233	2017.95	12.9	13.3	9	1
23403+1945	HO 302AB	29.4	0.016	79.86	0.037	2017.85	8.86	10.21	30	6
23432-0837	FOX 276AB	75.4	0.219	92.58	0.385	2017.87	9.72	11.30	2	1
23432-0837	FOX 276BC	251.6	1.412	5.11	0.139	2017.87	11.30	13.5	6	1
23479+1703	STF 3041A,BC	358.1	0.137	58.74	0.066	2017.89	8.35	8.36	5	1
23479+1703	STF 3041AB	358.6	0.098	56.73	0.107	2017.89	8.35	9.05	5	1
23479+1703	STF 3041AC	358.5	0.111	60.01	0.184	2017.89	8.35	9.18	5	1
23479+1703	STF 3041BC	356.3	0.115	3.33	0.235	2017.89	9.18	9.04	3	1
23525-0638	J 1427	143.6	0.759	6.31	0.113	2017.87	9.88	11.5	6	1
23525-0639	J 1428	223.0	1.743	8.86	0.263	2017.87	11.53	13.3	5	1
23546-2302	HJ 3225AB	342.5	0.612	30.92	0.332	2017.87	9.28	12.20	2	1
23574-1606	HJ 5435AB	7.7	0.923	14.58	0.241	2017.87	9.52	10.84	4	1
23574-1606	HJ 5435AC	52.3	0.686	23.68	0.264	2017.87	9.52	12.9	4	1
23574-1606	HJ 5435BC	90.3	0.824	17.10	0.382	2017.87	10.84	12.9	2	1
23592-3517	TDT4305	252.5	3.182	7.38	0.329	2017.87	11.12	12.31	2	1
23596-3151	BRT1834	68.6	2.669	6.55	0.255	2017.87	11.10	11.9	2	1
23597-3500	LDS6078AB	211.8	0.194	138.02	0.417	2017.87	9.14	9.87	2	1

Table 2 Notes:

- All magnitudes taken from the WDS catalogue. All PA and SEP measurements are for the Equator and Equinox of date.
- SEM – refers to standard error of the mean
- The column “samples” is the total number of observations made. “Nights” is the number of nights’ samples were collected for that system.

Continued from page 569

References

Daley, J., 2007, *JDSO,* **3** (4), 159-164.

Iverson, E. & Nugent, R., 2015, *JDSO*, **11** (2), 91-97.

Nugent, R. & Iverson, E., 2011, *JDSO*, **7** (3), 185-194.

Nugent, R. & Iverson, E., 2014, *JDSO*, **10** (3), 214-222.

Appendix 1

The following Avisynth script will allow *Limovie* to open a video file with enhanced video processing capabilities. Normally this file is placed in the same directory/folder with the video file. Simply re-type the script with a text editor but save it with the file extension ". avs". To open a video file select "AVI file open" button in *Limovie*, then click on "Files of type" and select the ".avs" file type.

The user needs to replace the bold text in the script with the relevant information for their situation. This includes giving the path and file name of the video file (first line). In Box 1 the user needs to provide their aspect ratio (variables **AW** and **AH**) and set the noise level (**NL**). The noise level range is 0-255 but the range of 25 ≤ **NL** ≤ 45 is typical. The video gain can be increased by decreasing the gain control (**GC**) setting. The range is 0-255 but typical settings are **GC** ≥ 70. The variable **TR** allows the user to vertically center the window on the target star by defining the top row of the segment. **TR** values are based on *Limovie*'s coordinate grid with the origin (0, 0) in *Limovie*'s upper left corner. For example, a TR = 50 means the top of the desired magnified segment will be 50 pixels down from the top of the video. See TR position in Figure 4 below. Care should be exercised so the bottom of the segment does not exceed the lower margin of the image.

The user must also select the magnification scale and the desired window (Box 2). To select a magnification scale and window just remove the # symbol from in front of the function call. A "#" designates anything to the right on that line as a comment and it is ignored by the program. If nothing is selected, the magnify function is disabled. Raising the noise floor helps eliminate background noise.

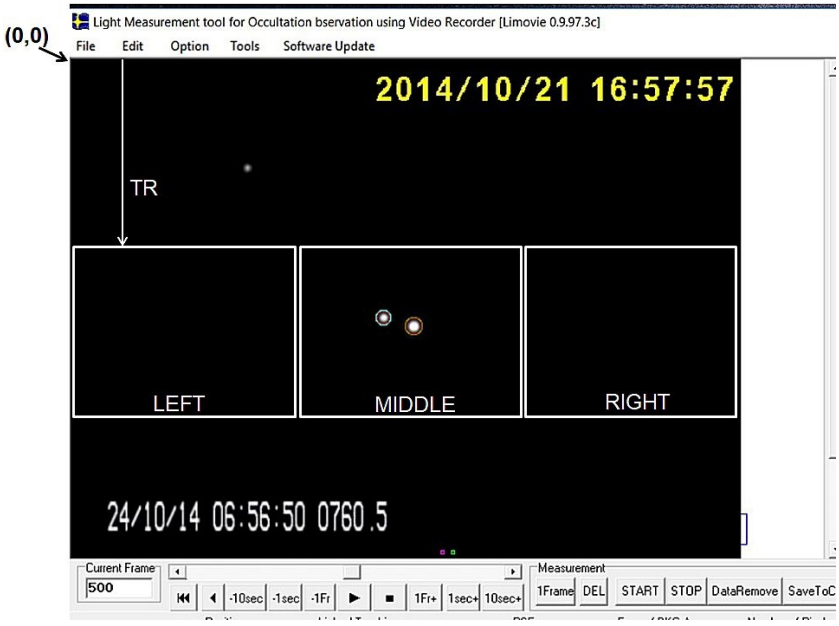

Figure 4. An example showing the origin of the Limovie coordinate system in the upper left corner of the image and how the TR variable relates to it. Limovie's frame counter is at the lower left corner.

Double Star Measures Using the Video Drift Method - XI

```
ClipMain = ("path to the desired video clip.avi")
DirectShowSource(ClipMain)

#    Box 1 - User Defined Input Settings

AW = 640      # enter aspect ratio width here
AH = 485      # enter aspect ratio vertical height here
NL =  25      # sets the noise floor, range 0-255
GC = 100      # acts like a gain control, range 0-255
TR =  50      # sets top row of segment (in Limovie's coordinate grid)

#    DO NOT CHANGE THE FOLLOWING SECTION
LanczosResize(AW, AH)    # sets the aspect ratio, do not move or make changes
A  = int(AW/2)
B  = int(AW/3)-1

#    Box 2 - User Defined Magnification and window Selection
#    Select the desired magnification scale and segment by removing the # symbol
#    in the first column.  Select only one function at a time.

#Magnify2x(AW, AH, TR, 0, -A)        # 2x magnification for left segment
#Magnify2x(AW, AH, TR, A, 0)         # 2x magnification for right segment

#Magnify3X(AW, AH, TR, 0, -B*2)      # 3x magnification for left segment
#Magnify3X(AW, AH, TR, B, -B)        # 3x magnification for middle segment
#Magnify3X(AW, AH, TR, B*2, 0)       # 3x magnification for right segment

#    DO NOT CHANGE THE FOLLOWING SECTION
Levels(NL,1,GC,0,255-NL,coring=false)    # sets the noise floor and apparent gain
Function Magnify2X(clip c, W, H, T, LX, LR)  {
YB = -H+(H/2+T)
Crop(c, LX, T, LR, YB)      # crops image
LanczosResize(W,H)          # expansion of cropped segment
}
Function Magnify3X(clip c, W, H, T, LX, LR)  {
YB = -H+(H/3+T)
Crop(c, LX, T, LR, YB)      # crops image
LanczosResize(W,H)          # expansion of cropped segment
}
```